A New Deformation Model of Hard α-Keratin Fibers at the Nanometer Scale: Implications for Hard α-Keratin Intermediate Filament Mechanical Properties

L. Kreplak,* A. Franbourg,† F. Briki,* F. Leroy,† D. Dallé,‡ and J. Doucet*

*Laboratoire pour l'Utilisation du Rayonnement Electromagnétique (LURE), Bât 209D, Centre Universitaire Paris-Sud, 91898 Orsay Cedex, †L'Oreal Recherche, 92583 Clichy Cedex, and ‡Laboratoire de Physique des Solides (LPS), Bât 510, Centre Universitaire Paris-Sud, 91405 Orsay Cedex, France

ABSTRACT The mechanical behavior of human hair fibers is determined by the interactions between keratin proteins structured into microfibrils (hard α-keratin intermediate filaments), a protein sulfur-rich matrix (intermediate filaments associated proteins), and water molecules. The structure of the microfibril-matrix assembly has already been fully characterized using electron microscopy and small-angle x-ray scattering on unstressed fibers. However, these results give only a static image of this assembly. To observe and characterize the deformation of the microfibrils and of the matrix, we have carried out time-resolved small-angle x-ray microdiffraction experiments on human hair fibers stretched at 45% relative humidity and in water. Three structural parameters were monitored and quantified: the 6.7-nm meridian arc, which is related to an axial separation between groups of molecules along the microfibrils, the microfibril's radius, and the packing distance between microfibrils. Using a surface lattice model of the microfibril, we have described its deformation as a combination of a sliding process and a molecular stretching process. The radial contraction of the matrix is also emphasized, reinforcing the hydrophilic gel nature hypothesis.

INTRODUCTION

Hard α-keratin fiber is a hierarchically structured material that shows a fibrillar organization from the micrometer to the nanometer scale (Zahn et al., 1980). The main part of the fiber, called the cortex, is composed of spindle-shaped cortical cells, about 100 μm long and 3 μm wide, which contain macrofibrils, 0.3 μm in diameter, glued together by an intermacrofibrillar matrix. A finest composite structure is found inside the macrofibril. It contains a two-dimensional (2D) array of cylindrical shaped units called the microfibrils (7.5 nm in diameter), embedded in a hydrophilic sulfur-rich protein matrix (Zahn et al., 1980). As for the other intermediate filaments (IFs), the microfibrils, or hard α-keratin IFs, are built from a complex axial and longitudinal assembly of heterodimers (Parry and Steinert, 1999). The heterodimer molecule, roughly 50 nm long, is characterized by a central rod domain composed of a double-stranded α-helical coiled coil interrupted by nonhelical segments. The central rod domain is surrounded by head and tail domains of unknown structure.

This extremely complex and well-defined structure gives rise to outstanding mechanical properties. Pushed by the textile industries, a large amount of work has been undertaken on wool, aiming at understanding the link between the fine microfibril-matrix texture and the macroscopic fiber properties (Feughelman, 1959). Nearly all the available models deal with the stress–strain curve of hard α-keratin fiber in water. Bendit (1960) described the molecular mechanism of microfibrils deformation as a gradual transition from α-helical coiled coils to β-sheet-like structures. Using this molecular mechanism as a basis, attempts were made to explain the elastic response of keratin fibers in terms of its two structural subcomponents, the microfibril and the matrix (Hearle, 2000). In Chapman's model (Chapman, 1969), matrix proteins are supposed to be covalently linked to fundamental repeat units aligned along the microfibril. The stress–strain curve of the fiber is modeled as a combination of the stress–strain curves of the microfibril and of the matrix in permanent interaction. This model is in good agreement with the mechanical experiments. Bendit and Feughelman (1968) have developed the so-called series zone model in which the microfibril contains two kinds of alternating zones, named X and Y, endowed with different elastic properties. The mechanical properties of the matrix are supposed to be driven by an entanglement of the matrix chains due to disulphide bonds. This model also reasonably fits the experimental data. More recently, another model based on the swelling properties of the matrix has been proposed by Feughelman (1994). In this model, water molecules are supposed to be ejected from the matrix at high stress levels, which leads to a matrix proteins compression between the microfibrils. Finally, Wortmann and Zahn (1994) have recently reinterpreted available biochemical data on the microfibril's structure to derive a model that neglects the matrix proteins. The X and Y zones of the series zone model are assigned to specific amino acid sequences along the length of the keratin molecule (Wortmann and Zahn, 1994).

These models are based on hypotheses, on the mechanical properties of the microfibril and of the matrix, and on their

Submitted June 25, 2001 and accepted for publication December 27, 2001.

Address reprint requests to Laurent Kreplak, Centre Universitaire Paris-Sud, LURE, Bât 209D-BP 34, 91898 Orsay Cedex, France. Tel.: +33-01-64-46-8834; Fax: +33-01-64-46-8820; E-mail: kreplak@lure.u-psud.fr.

0006-3495/02/04/2265/10 $2.00

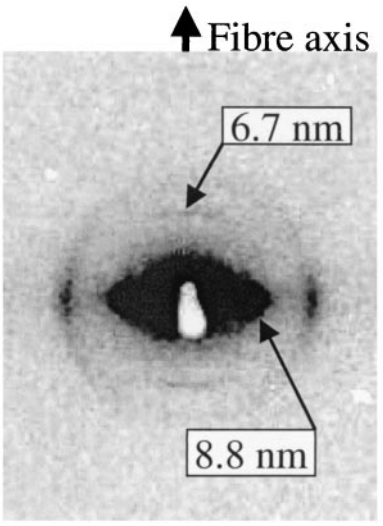

FIGURE 1 Typical SAXS pattern of hard α-keratin fiber (human hair). The 6.7-nm arc is visible along the fiber axis direction (meridian). Two broad peaks are visible perpendicular to the fiber axis (equator), one at 8.8 nm and the other one at 4.5 nm, which is superimposed to a ring because of the lipid granules scattering (Franbourg et al., 1995).

interactions, that are difficult to probe experimentally. Data on the mechanical deformation of the microfibril-matrix system at the nanometer scale can nevertheless be obtained using small-angle x-ray scattering (SAXS) on stretched α-keratin fibers.

The microfibril-matrix network gives rise to an intense and well-defined small-angle scattering pattern shown on Fig. 1

- In this study we have focused on the 6.7-nm arc along the meridian (fiber axis) which is related to an axial stagger between molecules or group of molecules along the microfibril (Fraser et al., 1986; Steinert et al., 1993).
- The three broad peaks at 8.8, 4.5, and 2.95 nm along the equator (plane perpendicular to the fiber axis) arise from the dense lateral packing of the microfibrils embedded in the matrix. The positions and the intensities of these peaks are characteristic of the microfibril diameter and of the mean center-to-center distance between microfibrils (Fraser et al., 1964). When the macroscopic fiber is immersed in water, the first peak position (8.8 nm) increases, indicating a matrix swelling (Fraser et al., 1971; Franbourg et al., 1995).
- Early attempts were made to study the deformation of this SAXS pattern in stretched α-keratin fibers. Wilson used several combinations of disulphide bonds reduction, silver staining, and fiber stretching in water to follow wool fiber modifications (Wilson, 1972). However the mechanical stretching effect could not be separated from the chemical treatments effects. The same kind of study has been performed for mohair fibers stretched in 2,2,2-trifluoroethanol (TFE) or in water (Spei, 1975). A striking displacement of the 6.7-nm arc was observed for the fibers in TFE, which follows the macroscopic strain until 40%. However this behavior was not observed in water. The main drawbacks of these works result from the use of chemical reagents, the need of fiber plaits and the need of long exposure times. The last point is particularly important because mechanical relaxation effects are likely to be accompanied by structural changes.
- To reduce relaxation effects, we have performed a time-resolved SAXS study on single human-hair fibers stretched at constant speed using a 5-μm-diameter beam. Two humidity conditions were selected to investigate the role of water, 45% relative humidity (RH) and immersed in water within a glass capillary.
- For the two humidity conditions, the 6.7-nm arc behavior has been monitored and analyzed using a surface lattice model of the microfibril (Fraser et al., 1976; Parry, 1995). The successive equatorial SAXS patterns have been analyzed using a fit procedure developed by Briki et al. (1998). Equatorial SAXS pattern analysis allowed following of two parameters of the microfibril-matrix network, the radius of a cylindrically averaged microfibril, and the mean center-to-center distance between microfibrils assuming a pseudohexagonal packing.
- Using these data, we have been able to characterize the local deformability of the two components at the two humidity conditions. The matrix has been shown to withstand a high lateral contraction at 45% RH and in water. The microfibril behavior is more complex, it is characterized by a much lower lateral compressibility than the matrix and by a deformability of its axial internal structure, which is water-content dependent. On the basis of these results and of biochemical data on keratin filament assembly, we propose a model of the microfibril internal deformation in which the keratin molecules are submitted to a molecular stretching coupled with a sliding process, favored by water, which retains some features of the microfibril's internal structure.

MATERIALS AND METHODS

Samples

Data collections were carried out on virgin Caucasian human hair samples. The samples, approximately 0.07 mm in diameter, were analyzed at 24 $\pm$ 0.5°C (room temperature) and at two humidity conditions, 45 $\pm$ 2% RH (room humidity) and in a glass capillary filled with water.

Mechanical set-up

A specific uniaxial extensometer compatible with synchrotron x-ray diffraction set-ups has been designed for this experiment. With such extensometer, the fiber's central zone is stretched without any displacement and can be analyzed by x-ray diffraction without moving the beam.

The apparatus is composed of two L-shaped pieces aligned on a motorized bench and each supporting a clamp to hold the sample horizontally. A transducer is used to move simultaneously the two clamps; an electronic

device has been developed to pilot the transducer and to ensure a one micrometer accuracy on the displacement. Because this apparatus is designed to be used with a microdiffraction set-up, particular attention has been paid to ensure that the position of the sample does not change vertically during stretching.

The native length of the samples was fixed to 30 mm. A constant stretching speed of 2% of the initial length per minute has been applied to the samples until failure. These conditions are matching the ones used in textile fibers standard tensile tests (ASTM, 1982).

X-ray scattering set-up

Experiments were carried out at the European Synchrotron Radiation Facility on the microfocus beamline ID13 (Lichtenegger et al., 1999; Riekel et al., 2000). A high-intensity monochromatic beam from an undulator (wavelength $\lambda = 0.0948$ nm) was focused and then size-limited down to a 5-μm-diameter circular section by a collimator. Single hair fibers were mounted horizontally on the stretching apparatus described above. The stretching apparatus was installed on a computer-controlled Physike Instrument's X/Y stage with the stretching direction perpendicular to the x-ray beam. The stage was coupled to a microscope that permitted sample positioning with 0.1-μm accuracy. The sample detector distance was 161 mm, it was measured using silver behanate (first-order spacing: 5.838 nm). Small-angle x-ray scattering patterns were recorded on a MAR CCD camera (2048 $\times$ 2048 pixels) with a pixel size of (0.06445 $\times$ 0.06445 mm^2). All the diffraction patterns have been recorded with an exposure time of 30 s. This exposure duration has been checked to induce no damage on an unstretched fiber.

The samples were vertically positioned in such a way that the beam passes along their diameter. A deformation of 1% of the original length was integrated during each 30-s exposure. SAXS patterns were taken at times 0, 60, 150, 300 s, and then every 150 s until fiber failure. These times correspond to strains of 0, 2, 5, 10%, and then every 5% of the original length. To avoid radiation damage, the x-ray beam was moved by 20 μm along the fiber axis between two exposures. Interestingly for an unstretched hair fiber, it has been demonstrated in a previous study that the SAXS pattern does not change at the millimeter scale along the fiber length (Baltenneck et al., 2000).

Data Treatment

For each SAXS pattern, the air- or the water-filled capillary contributions was subtracted using a pattern that was collected just above the sample surface. One-dimensional (1D) meridian and equatorial profiles passing through the origin were extracted from the 2D patterns by integrating the intensity on a 20-pixels-thick rectangular strip.

Equatorial intensity modeling

The 1D equatorial profiles $I(S)$, with S the scattering vector modulus, have been modeled using the following expression derived from Briki et al. (1998):

$$I(S) = I_0(S) + Z(S) \times |F(S)|^2 \qquad (1)$$

$I_0(S)$ is a small-angle background that can be modeled as a power law $B_1S^{-2.3} + B_2$. $Z(S)$ is the interference function of the 2D microfibril-matrix lattice. $F(S)$ is the form factor of the microfibril cross-section.

The interference function Z(S)

In this model, the microfibril-matrix network is described as a hexagonal 2D paracrystal. The advantage of the paracrystal description lies in the analytical derivation of $Z(S)$. In our case, $Z(S)$ calculation has been performed according to Busson and Doucet (2000), assuming a hexagonal packing of microfibrils. We use a set of 1D $Z(S)$ profiles extracted from 2D interference function maps. The damping and the width of the peaks depend on the standard deviation σ of the distribution between first neighbors expressed as a percentage of the average hexagonal lattice length noted, A_m. Note that the first peak of $Z(S)$ corresponds to the first peak on the experimental profiles and its position is directly related to the value of A_m (Briki et al., 1998).

The microfibril form factor F(S)

It is the scattered amplitude by an isolated microfibril of electron density $\rho(\mathbf{r})$, with $\mathbf{r}$ the position vector. Because the microfibril is a cylindrical-shaped object, we only consider 1D functions $\rho(r)$ and $F(S)$. For low resolution data, it is not necessary to consider the whole set of individual atomic positions. The microfibril can be simply described as an infinitely long, axially uniform cylinder. Because of the uniformity of the density along the cylinder axis, the scattered amplitude $F(S)$ is different from zero only on the equatorial plane. Then we get the well-known expression,

$$F(S) = 2\pi\Delta\rho R^2 J_1(u)/u \quad \text{with} \quad u = 2\pi RS. \qquad (2)$$

$\Delta\rho$ is the electron density contrast between the microfibril and the surrounding matrix, and R is the cylinder's radius. A_m, R, σ, $\Delta\rho$, B_1, and B_2 are adjusted during the fitting procedure. Three parameters, A_m, R, and σ, describe the microfibril-matrix network. They determine the peaks shape and position for the fitting curve. The other three parameters, $\Delta\rho$, B_1, and B_2, are only used to fit the intensity. For each data set, the experimental intensity profile at 0% macroscopic strain was fitted using the model described above. For the other macroscopic strains, the R and A_m values were allowed to vary, whereas σ value has been fixed to 32.5%. The sensitivity of this fitting procedure to the three main parameters' variation was estimated to $\pm$2.5% on σ and $\pm$0.025 nm on R and A_m.

Interpretation of the 6.7-nm meridian arc using a surface lattice model and biochemical data

To give a molecular interpretation of the 6.7-nm meridian arc origin, we have chosen to describe the microfibril's supramolecular assembly using a surface lattice model (Parry and Steinert, 1999). Figure 2 shows the microfibril surface lattice model proposed by Fraser et al. (1986) on the basis of porcupine quill's x-ray scattering pattern. This lattice, which corresponds to a 2D unfolding of the cylindrical microfibril architecture, contains seven rows, for which the molecular origin will be presented below. To account for the x-ray diffraction data, the lattice contains a helical dislocation characterized by a unit height of 47 nm, a unit twist of 49.1°, and a pitch length of 344.7 nm (Parry, 1995). The two other main parameters of this model are the axial projections Z_a and Z_b of the two lattice vectors a and b (Fig. 2). Experimentally, the 6.7-nm meridian arc can be considered as a direct image of Z_a, and Z_b corresponds roughly to the 20-nm periodicity observed on transmission electron microscopy images of stained intermediate filaments (Milam and Erickson, 1982).

At the molecular level, a tetrameric unit obtained by the axial staggering of two dimeric molecules (Herrmann and Aebi, 1998) is located on each lattice point and thus each lattice row (Fig. 2 *a*) contains one tetrameric unit in cross-section and is named a protofilament. The existence of the protofilament as a stable intermediate between the tetrameric unit and the full-length intermediate filament is a well-admitted hypothesis that is consistent with some electron microscope data (Aebi et al., 1983). Cross-linking studies on various IF systems have shown that only four modes of molecule alignments within the tetrameric unit coexist in the IF structure, they are named A_{12}, A_{11}, A_{22}, and A_{CN}. The corresponding axial staggers

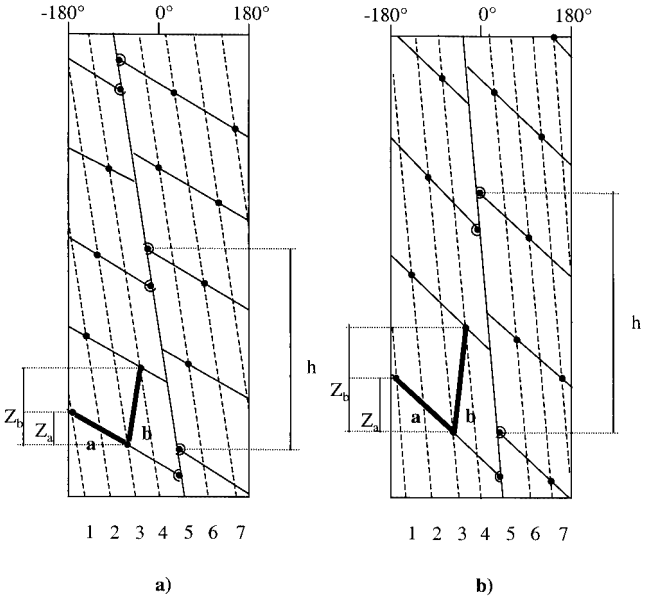

FIGURE 2 (*a*) The surface lattice model of hard α-keratin intermediate filament with 7 protofibrils (*dotted lines*) (Parry and Steinert, 1999). The parameter *h* is the unit height of the lattice helical dislocation. Z_a and Z_b are the axial projections of the two lattice vectors a and b. Z_a is the axial distance between consecutive lattice points. Z_b is the axial distance between lattice points in adjacent protofibrils. (*b*) The same model for a hard α-keratin intermediate filament stretched arbitrarily along the fiber axis. Z_a was increased by 77%, Z_b was increased by 36%, and *h* was increased by 19%.

can be determined for each mode of assembly (Table 1) and are summarized in Fig. 3 (Steinert et al., 1993).

A molecular lattice model of the hard α-keratin microfibril has been proposed by Parry using a geometrical lattice described above and the cross-linking data available for soft α-keratin IF (Steinert et al., 1993). To relate the surface lattice parameters Z_a and Z_b with the axial staggers obtained from cross-linking studies, Parry has derived the relationships (Parry, 1995),

$$Z_a = A_{11} + A_{22} - 2A_{12}, \quad (3)$$

$$Z_b = A_{12} - A_{11}. \quad (4)$$

TABLE 1 Axial parameters for oxidized and reduced hard α-keratin intermediate filament and soft α-keratin intermediate filament

Parameters (nm)	Hard α-keratin		Soft α-keratin†
	Ozidized*	Reduced*	
A_{CN}	−2.54	0.003	1.01
A_{11}	−19.96	−17.44	−16.58
A_{12}	0.5	0.41	0.06
A_{22}	27.53	27.52	28.63
Z_a	6.55	9.26	11.93
Z_b	20.4	17.85	16.64

Z_a and Z_b values have been deduced using Eqs. 3 and 4.
*Wang et al. (2000).
†Steinert et al. (1993).

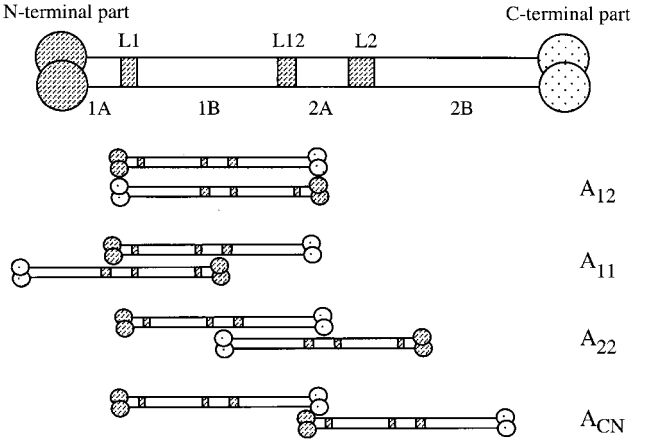

FIGURE 3 The four assembly modes of two keratin molecules within the tetrameric unit of intermediate filaments. L1, L12, and L2 are the links between the four coiled coil domains 1A, 1B, 2A, and 2B (Parry and Steinert, 1999).

These relationships can be used to link the behavior of the 6.7-nm meridian arc with the behavior of three of the four modes of molecules assembly within IF.

Finally, one should notice that the number of chains in cross-section of the microfibril is not yet firmly established. Based on x-ray diffraction measurements, Fraser et al. (1969) proposed 26–28 chains (almost 7 protofibrils), whereas, more recently, Jones et al. (1997) proposed 30–32 chains (almost 8 protofibrils) from scanning transmission electron microscopy observations. However, the above-described relationships (Eqs. 3 and 4), that relate different staggers within the microfibril are not dependent on the number of protofibrils.

RESULTS

Behavior of the 6.7-nm meridian arc

Upon stretching the fiber, all the meridian reflections are shifted toward small angles of diffraction. Above 5% macroscopic strain, most of the sharp reflections characteristic of the microfibril long-range order are disappearing, and only the dominant 6.7-nm arc remains present (Kreplak et al., 2001).

The position of the 6.7-nm meridian arc is almost insensitive to humidity variations (Franbourg et al., 1995). During mechanical stretching, the position shifts continuously toward higher values, but the arc intensity behaves differently according to the humidity (Fig. 4). At 45% RH, the arc displacement is coupled with a rapid intensity decrease and a lateral broadening of the reflection. At 15% macroscopic strain, the arc position has reached 7.7 nm. Above 15% macroscopic strain, the arc completely disappeared. In water, the arc displacement occurred until fiber failure at 40% macroscopic strain and the arc intensity decreased slowly with almost no lateral broadening. At 35% macroscopic strain, the arc position reached 9.6 nm.

It is worth noting that the spacing displacement is never equal to the corresponding macroscopic strain (Fig. 4). The

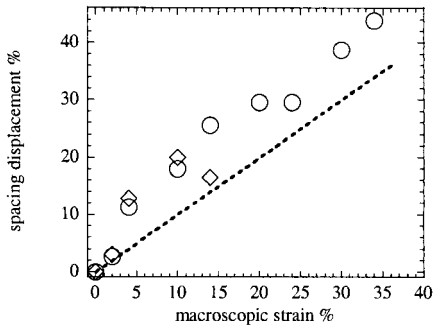

FIGURE 4 Relative displacement of the meridian 6.7-nm arc as a function of macroscopic strain for the two humidity conditions, 45% RH (*diamonds*) and water (*circles*). The dotted line corresponds to the macroscopic strain.

macroscopic and the microscopic deformation have a common tendency but cannot be compared directly. This can be due to a modification of the hair ultrastructure like, for example, a macrofibril slippage. However, a macrofibril slippage cannot at all explain the behavior of the 6.7-nm arc, which is related to the microfibril structure inside the macrofibril.

Modification of the equatorial SAXS pattern

The 1D equatorial profiles of an unstretched human hair fiber at 45% RH and in water are shown in Fig. 5 *a*. The position of the first peak is clearly shifted toward small angles when the fiber is immersed in water as previously documented by other researchers (Briki et al., 1998; Franbourg et al., 1995; Fraser et al., 1971).

At both humidity conditions, the peaks of the equatorial intensity profile were shifted to higher scattering angles upon stretching the fiber. This is illustrated in Fig. 5 *b* with two equatorial profiles of a human hair fiber unstretched and stretched to 25% macroscopic strain, at 45% RH.

The fitting procedure described above has been used on the two sets of profiles, at 45% RH and in water. The first (0% strain) and last (35% strain) profiles of the set in water are shown on Fig. 6, *a* and *b*, respectively. For both data sets, the values of the mean hexagonal lattice length A_m and the microfibril's radius R, deduced from the fitting procedure, have been plotted, as a function of macroscopic strain, in Figs. 7 and 8, respectively.

The initial value of the mean hexagonal lattice length A_m is dependent on the fiber's water content. At 45% RH, A_m is equal to 8.68 nm and its value reaches 10 nm in water. During stretching, A_m decreases as shown in Fig. 7. For the two humidity conditions, just before fiber failure, A_m value is equal to 85% of its initial value.

The initial value of the microfibril's radius R is weakly dependent on the fiber's water content. When stretching the fiber, R decreases as shown in Fig. 8, with a behavior that is extremely dependent on RH. The decrease occurred above 5% macroscopic strain at 45% RH and above 15% macroscopic strain in water. Just before fiber failure, R value is equal to 93% of its initial value at 45% RH, and to 96% of its initial value in water.

DISCUSSION

The main and striking result from the present study is the observation of a large increase in the microfibril's axial separation between groups of molecules when a hard α-keratin fiber is stretched in water at constant speed. We will first discuss the special conditions necessary to observe this behavior. Second, we will analyze the data about the axial and lateral behavior of the microfibril using the surface lattice model described above. A supramolecular model of

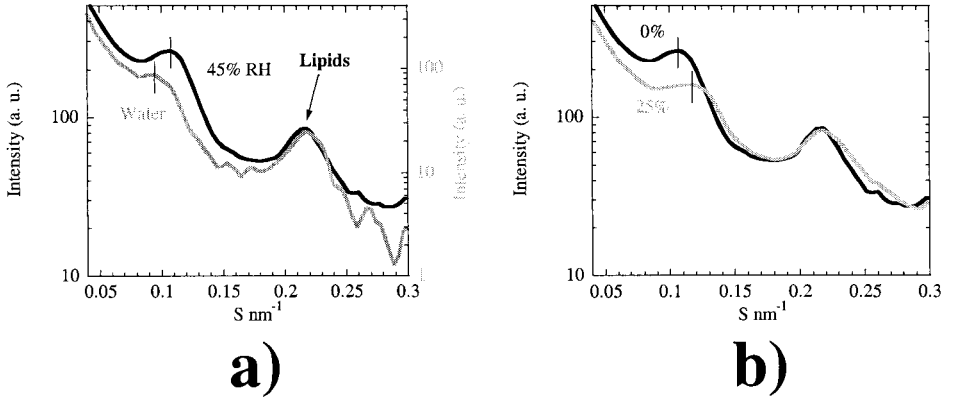

FIGURE 5 (*a*) One-dimensional equatorial intensity profiles extracted from the SAXS patterns of unstretched human hair fibers at 45% RH (*black curve*) and in water (*gray curve*). The dotted lines are drawn to show the shift of the first peak. (*b*) One-dimensional equatorial intensity profiles extracted from the SAXS patterns of the human hair fiber continuously stretched at 45% RH; *black curve*, 0% macroscopic strain; *gray curve*, 25% macroscopic strain. The dotted lines are drawn to show the shift of the first peak.

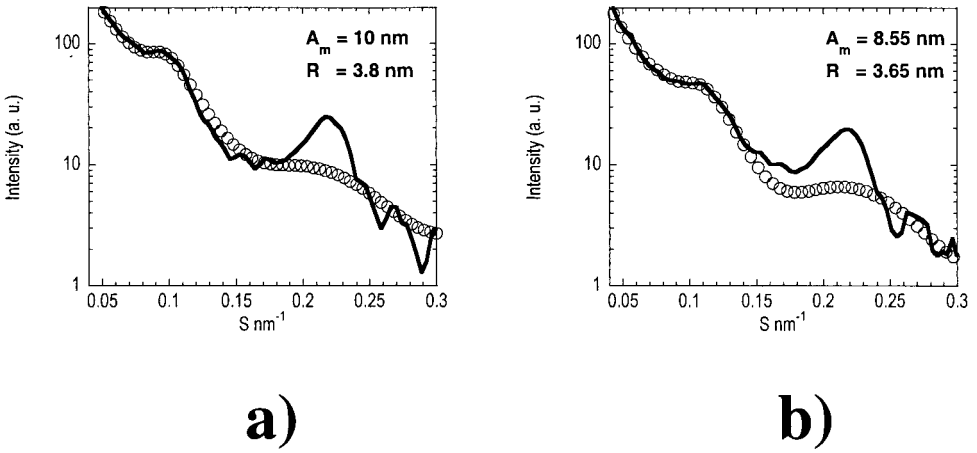

FIGURE 6 One-dimensional equatorial intensity profiles extracted from the SAXS patterns of the human hair fiber continuously stretched in water. (*a*) *Solid curve*, experimental profile at 0% macroscopic strain; *circles*, intensity modeling derived from Eq. 1. (*b*) *Solid curve*, experimental profile at 35% macroscopic strain; *circles*, intensity modeling derived from Eq. 1.

the microfibril deformation will be presented. Third, the role of water will be discussed using the above model. Finally, our data will be used to derive a mechanical model of the matrix.

Relaxation effects in hair fiber

In earlier studies, it had been shown that the position of the 6.7-nm meridian arc could be increased by 40% when mohair fibers were stretched in 2,2,2-trifluoroethanol. In water, the displacement of the arc was only ~5% (Spei and Zahn, 1971; Spei, 1975). To get good quality SAXS patterns, it was necessary to use fiber plaits and long exposure times (at least one hour), allowing the fibers to relax. Such relaxation process, which is associated with a stress decay (Peters and Woods, 1956), could affect the structure of both the microfibril and the matrix. Consequently, those results were probably biased by structural relaxation processes. Our different results concerning the displacement of the 6.7-nm meridian arc confirm this hypothesis.

In the present experimental set-up, the fiber was continuously stretched during the SAXS measurements because data collection only required 30 s. By avoiding the relaxation of the fiber in water, we have been able to observe the true behavior of the 6.7-nm arc upon stretching (see Fig. 4). It appears that time-resolved studies are absolutely necessary to reveal the behavior of both the microfibril and the matrix during a standard tensile test.

A supramolecular model of the microfibril mechanical deformation

We aim to understand how the microfibril can withstand the large increase of its axial separation between groups of molecules (Fig. 4), while being only slightly radially contracted (Fig. 8). Considering the microfibril as a homogenous cylinder is obviously a crude approximation, it is

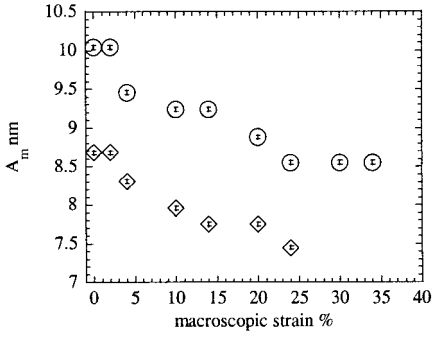

FIGURE 7 The mean center to center distance between microfibrils A_m as a function of macroscopic strain, 45% RH (*diamonds*), water-filled capillary (*circles*). For the two humidity conditions, the values of A_m were obtained from the intensity modeling described in the text.

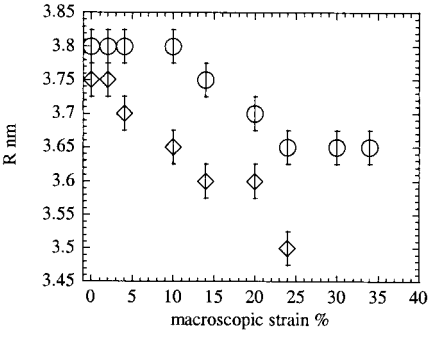

FIGURE 8 The microfibril radius *R* as a function of macroscopic strain, 45% RH (*diamonds*), water (*circles*). For the two humidity conditions the values of *R* were obtained from the intensity modeling described in the text.

necessary to consider the molecular and supramolecular architectures.

Intensive research efforts have been made to study the stretching effects on the structure of the double stranded α-helical coiled coils, which form the core of the keratin molecule, inside the microfibril (Spei and Holzem, 1987). It is now well admitted that, when stretching the macroscopic fiber, the coiled coils undergo conformational changes that lead to a disordered (Skertchly and Woods, 1960) or β-sheet-like (Bendit, 1960) structure, depending on the macroscopic strain and on the humidity conditions (Kreplak et al., 2001). However, these conformational changes of the keratin molecules cannot fully explain the mechanical "response" of the microfibril/matrix network.

We have based our study on the analysis of the 6.7-nm meridian arc. First, we have measured the lateral width of this reflection. Our measurements at rest lead to a value of $0.11–0.14\ \mathrm{nm}^{-1}$, which corresponds to coherent lengths of 7–9 nm. This range includes the value of the microfibril diameter (7.5 nm), which proves that the 6.7-nm reflection arises from the microfibril internal structure and not from a group of microfibrils. Under stretching, the coherent length slightly decreases down to 5 nm, which further confirms the intramicrofibrillar origin of the 6.7-nm arc. These results clearly show that the coiled coil mechanical "response" is linked, in fact, to structural changes occurring inside a given microfibril.

To qualify these changes, we used the surface lattice model described in the section, The Interference Function $Z(S)$, to relate the 6.7-nm meridian arc to the hard α-keratin molecules' axial stagger Z_a within the microfibril (Fig. 2). So the huge increase in the 6.7-nm arc position shown in Fig. 4 can be interpreted as an increase in this stagger arising from a sliding of the keratin molecules along the microfibril axis. However, this sliding process must occur in such a way that the internal microfibril structure remains well defined, because the 6.7-nm arc intensity does not decrease (at least in water). Going further in the interpretation requires consideration of the cross-linking study on hard α-keratin intermediate filaments, either oxidized or reduced (Wang et al., 2000).

Recently, Wang et al. (2000) have performed cross-linking experiments on hard α-keratin intermediate filaments assembled in vitro in oxidative and reductive buffers, using hard α-keratin proteins extracted from mouse hair fibers. Their results on the four axial staggers A_{12}, A_{11}, A_{22}, and A_{CN} are summarized in Table 1 for the two buffer conditions. In going from the reductive to the oxidative buffer, A_{12}, A_{22} and the keratin molecule lengths are kept almost constant, but A_{11} decreases by roughly 2.5 nm (Table 1).

In this study, we have used Wang et al.'s data in Eqs. 3 and 4 to calculate the Z_a and Z_b values for the two surface lattice models of the hard α-keratin filament in the oxidized and reduced states. We get $Z_a = 6.55$ nm and $Z_b = 20.4$ nm for the oxidized filaments, and, for reduced filaments, values $Z_a = 9.26$ nm and $Z_b = 17.85$ nm. Therefore, Z_a increases by roughly 40% between the oxidized and the reduced state. In contrast, Z_b decreases from the oxidized to the reduced state. This decrease is directly related to the intermediate filament shortening (Wang et al., 2000).

We reveal, with the present data, a striking similarity between the behavior of the position of the 6.7-nm meridian arc when a human hair fiber is stretched in water (see section 3.1.1) and the behavior of Z_a for oxidized and reduced hard α-keratin filaments deduced from cross-linking data. Changing only one axial stagger characteristic of the hard α-keratin IF structure (A_{11}) can account for the huge displacement of the 6.7-nm meridian arc during continuous mechanical stretching of a hair fiber in water. However, in our experiments, the increase in Z_a is induced by the microfibril mechanical stretching, whereas, in the cross-linking experiment, it is associated with a shortening of the microfibril. Then it is most likely that the sliding process involves the four assembly modes (A_{11}, A_{12}, A_{22}, A_{CN}), which are coupled, to mechanically stretch the microfibril without disordering its structure. Such a mechanism would induce an increase in the three surface lattice parameters, h, Z_a, and Z_b in a way similar to the one shown in Fig. 2 *b*.

It is important to notice the existence of interchain disulphide bonds between keratin molecules within the microfibril (Wang et al., 2000). If these bonds were not broken, they could hamper the sliding process during stretching and induce a stretching of the keratin molecules. Then it is important to understand that two dynamic processes are in competition, a molecular stretching and a molecular sliding that is coupled with the breakage of some disulphide bonds. The key parameter is the energetic balance between the two processes, and this balance is certainly sensitive to a wide range of parameters, including stretching speed, temperature, and RH (see the following discussion). Because we have no simple way to measure accurately the energetic cost of each process, we are basing our analysis on a simulation done for model α-helices. Recently, a molecular mechanics approach by Rhos et al. (1999) has shown that a longitudinal shearing of two α-helices along their axis (sliding process) is energetically more favorable than the mechanical unraveling of one α-helix. In our case, we have to deal with coiled coils interfaces and not simply with two parallel α-helices, however this result indicates that coupling disulphide bonds breakage with a molecular sliding process could be more favorable than a pure molecular stretching.

The sliding or shearing process that has been discussed above may neither imply a change of the microfibril's radius R nor a stretching of the keratin molecules. In fact, the slight microfibril's radius decrease that is observed in this study (Fig. 8) indicates a contribution from another mode of microfibril deformation. Considering that wide-angle x-ray scattering experiments have clearly demonstrated the existence of a molecular stretching process within the microfibril (Bendit, 1960; Kreplak et al., 2001),

it is straightforward that this process is associated with the sliding process described in this study.

The role of water in the mechanical behavior of the microfibril

When a hair fiber is stretched in water, the main deformation process of the microfibrils is the internal sliding process described above. Our experimental data (Fig. 4) prove that a microfibril embedded in a water-swollen matrix can withstand a high amount of shear without loosing its supramolecular order, because the 6.7-nm arc can reach a 9.6-nm position without disappearing. Such a huge displacement can only be obtained by a sliding process of the keratin molecules with respect to the four modes of interactions A_{12}, A_{11}, A_{22}, and A_{CN} introduced above. However, these modes of interactions are dependent on the complex pattern of positively and negatively charged residues located at the surface of the keratin molecule. Such three-dimensional charge distribution is supposed to play a role in the formation and stability of intermediate filaments through ionic interactions (Meng et al., 1994; Mehrani et al., 2000).

In this context, the main role of the water molecules present inside and around the microfibril should be to screen the charges, resulting in a decrease of the sliding-process energy cost. This may explain why the microfibril elongates in water without losing its internal structure below 40% macroscopic strain. Because of our stretching frame, higher strain values could not be reached, the limit is generally 60% macroscopic strain (Morton and Hearle, 1993; Meredith, 1956). However, we believe that, between 40 and 60% macroscopic strain, the molecular stretching process will predominate.

On the contrary, at 45% RH, the amount of water molecules that are present inside and around the microfibril should not be high enough to screen the charges, limiting the amplitude of the sliding process. In that case, the deformation process mainly involves a molecular stretching leading to a total disordering of the microfibril internal structure. The disordering of the keratin molecular structure has already been analyzed in detail, using wide-angle x-ray scattering, for horse hair fibers stretched at 30% RH (Kreplak et al., 2001).

This study shows clearly that the mechanical behavior of the microfibril results from the combination of two processes that occur at different levels. The first process is a stretching of the keratin molecules, which may be related to the unraveling of the coiled coils (Kreplak et al., 2001) or to the α-helix–β-sheet transition proposed by Bendit (Bendit, 1960). The second process that occurs at the supramolecular level is the keratin molecules sliding along the microfibril axis. At 45% RH the two modes of deformation are combined, whereas, in water, the sliding process predominates at least until 40% macroscopic strain.

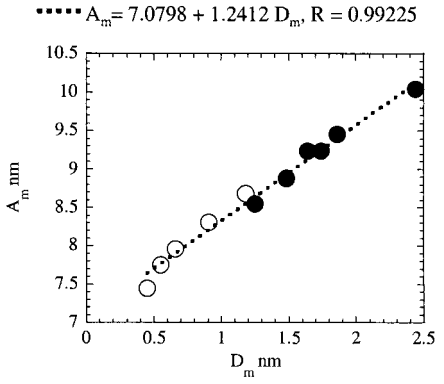

FIGURE 9 The mean center-to-center distance between microfibrils A_m as a function of $D_m = A_m\text{-}2R$, for the two humidity conditions, 45% RH (*open circles*) and water (*filled circles*). The dotted line is a linear least square fit.

Some aspects of the mechanical properties of the matrix

From experimental results on the behavior of the mean center-to-center distance between microfibrils A_m (Fig. 7), it is possible to deduce some information about the mechanical properties of the sulfur-rich matrix. A structural parameter that is characteristic of the matrix is the closest edge-to-edge distance between microfibrils noted D_m. D_m is equal to $A_m\text{-}2R$. The plot of A_m versus D_m is shown on Fig. 9 for the two humidity conditions. It is clear from this plot that A_m and D_m are linearly related to each other with a slope around one. This remark proves that the microfibril plays a minor role in the contraction of the microfibril-matrix network. The decrease of A_m with respect to the applied macroscopic strain is thus simply related to the matrix lateral contraction. The value of A_m is directly linked to the position of the first peak on the equatorial SAXS pattern (Fig. 1), indicating that, in first approximation, the matrix lateral contraction can be simply measured by following the displacement of the first equatorial peak without any complex intensity modeling. This result could be helpful to analyze the matrix response under various mechanical and chemical stresses.

To characterize accurately the lateral behavior of the matrix, we can estimate from our data the surface of matrix S_{mat} associated with a microfibril in the pseudo hexagonal lattice:

$$S_{mat} = \frac{A_m^2 \times \sqrt{3}}{2} - \pi R^2. \quad (5)$$

The results are shown on Fig. 10 for the two humidity conditions. It is noteworthy that, in water, the surface of matrix is multiplied by 2. The initial value of S_{mat} is divided by 2 just before fiber failure for the two humidity conditions. The matrix is thus submitted to a huge lateral contraction upon stretching the hair fiber. In other words, the

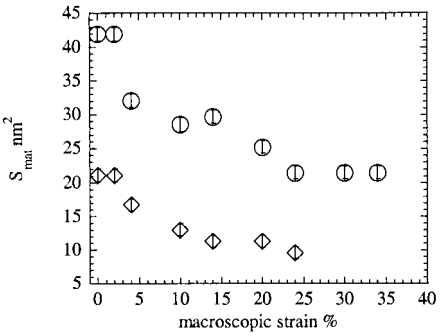

FIGURE 10 The surface of matrix S_{mat} associated with a microfibril in the pseudo hexagonal lattice (see Eq. 5) as a function of macroscopic strain for the two humidity conditions, 45% RH (*diamonds*), water (*circles*).

surface fraction of microfibrils in the network increases from 67 to 80% at 45% RH and from 50 to 66% in water. These data clearly emphasize the fact that the matrix is a highly deformable material that can swell in water or contract strongly under a mechanical stress. Such behavior seems consistent with an hydrophilic gel behavior of the matrix. That the microfibril surface fraction increases upon stretching indicates that the microfibril-matrix network is a highly heterogeneous composite in which stress localization may occur.

CONCLUSION

Combining time-resolved SAXS and mechanical stretching of hard α-keratin fiber, we have analyzed the supramolecular deformation of the microfibril-matrix network. We have been able to characterize the mechanical behavior of each of the two components separately. We have shown that the mechanical stretching of the microfibril involves a combination of two processes, a stretching of the keratin molecules and a sliding of these molecules inside the microfibril. The importance of these two processes is water-content dependent; when the hair fiber is stretched in water, the sliding process predominates, whereas, at 45% RH, the combination of both processes leads to a "melting" of the microfibril supramolecular structure. The huge lateral contraction of the matrix under an axial stretching has been attributed to a hydrophilic gel behavior of this component.

Our results emphasize the complex microscopic processes that underlie the macroscopic deformation of hard α-keratin fibers as a function of humidity. The mechanical properties of the fiber cannot be simply related to its native microscopic structure. The present data could be used as constraints in a computer modeling of the mechanical properties of the microfibril-matrix network, similar to the one developed for the analysis of spider silk mechanical properties (O'Brien et al., 1998). We would also like to point out that the sliding mechanism described above is certainly one of the clues that permit understanding of the creep and relaxation properties of hair fibers (Peters and Woods, 1956)

The authors would like to thank especially M. Müller from the European Synchrotron Radiation Facility, ID13 beamline, were all the experimental measurements were performed.

The stretching apparatus described in the section, Mechanical Set-up, has been developed in the Service de Mécanique of the Laboratoire de Physique des Solides (Orsay, France). The authors would like to thank, P. Aymard for the conception of all the electronic devices that pilot the apparatus and B. Kasni for the apparatus fabrication.

REFERENCES

Aebi, U., W. E. Fowler, P. Rew, and T. T. Sun. 1983. The fibrillar substructure of keratin filaments unraveled. *J. Cell Biol.* 97:1131–1143.

American Society for Testing and Materials. 1982. Standard test method for tensile properties of single textile fibers. Designation: D3822 - 82. *In* Annual book of ASTM standards. A. S. f. T. a. Materials, Philadelphia, PA.

Baltenneck, F., J. C. Bernard, P. Garson, C. Engstrom, F. Riekel, A. Leroy, Franbourg, and J. Doucet. 2000. Study of the keratinization process in human hair follicle by X-ray microdiffraction. *Cell Mol. Biol. (Noisy-le-grand).* 46:1017–1024.

Bendit, E. G. 1960. A quantitative x-ray diffraction study of the alpha-beta transformation in wool keratin. *Text. Res. J.* 30:547–555.

Bendit, E. G., and M. Feughelman. 1968. Keratin. *Encycl. Polymer Sci.* 8:1–44.

Briki, F., B. Busson, and J. Doucet. 1998. Organization of microfibrils in keratin fibers studied by x-ray scattering modelling using the paracrystal concept. *Biochim. Biophys. Acta.* :57–68.

Busson, B., and J. Doucet. 2000. Distribution and interference functions for two-dimensional hexagonal paracrystals [In Process Citation]. *Acta Cryst. A.* 56:68–72.

Chapman, B. M. 1969. A mechanical model for wool and other keratin fibers. *Text. Res. J.* :1102–1109.

Feughelman, M. 1959. A two-phase structure for keratin fibers. *Text. Res. J.* :223–228.

Feughelman, M. 1994. A model for the mechanical properties of the alpha-keratin cortex. *Text. Res. J.* 64:236–239.

Franbourg, A., F. Leroy, J. L. Lévêque, and J. Doucet. 1995. Influence of water on the structure of α- keratin fibres. *In* 5th International Conference on Biophysics and Synchrotron Radiation, Grenoble, France, .

Fraser, R. D. B., T. P. MacRae, and A. Miller. 1964. The coiled coil model of alpha-keratin structure. *J. Mol. Biol.* 10:147–156.

Fraser, R. D. B., T. P. MacRae, G. R. Millward, D. A. D. Parry, E. Suzuki, and P. A. Tulloch. 1971. The molecular structure of keratins. *Appl. Polym. Symp.* 18:65–77.

Fraser, R. D. B., T. P. MacRae, D. A. D. Parry, and E. Suzuki. 1969. The structure of beta-keratin. *Polymer.* 10:810–826.

Fraser, R. D. B., T. P. MacRae, D. A. D. Parry, and E. Suzuki. 1986. Intermediate filaments in alpha keratins. *PNAS.* 83:1179–1183.

Fraser, R. D. B., T. P. MacRae, and E. Suzuki. 1976. Structure of the alpha-keratin microfibril. *J. Mol. Biol.* 108:435–452.

Hearle, J. W. 2000. A critical review of the structural mechanics of wool and hair fibres. *Int. J. Biol. Macromol.* 27:123–138.

Herrmann, H., and U. Aebi. 1998. Intermediate filament assembly: fibrillogenesis is driven by decisive dimer–dimer interactions. *Curr. Op. Struct. Biol.* 8:177–185.

Jones, L. N., M. Simon, N. R. Watts, F. P. Booy, A. C. Steven, and D. A. D. Parry. 1997. Intermediate filament structure: hard alpha keratin. *Biophys. Chem.* 68:83–93.

Kreplak, L., J. Doucet, and F. Briki. 2001. Unraveling double stranded alpha-helical coiled coils: an x-ray diffraction study on hard alpha-keratin fibers. *Biopolymers.* 58:526–533.

Lichtenegger, H., M. Müller, O. Paris, C. Riekel, and P. Fratzl. 1999. Imaging of the helical arrangement of cellulose fibrils in wood by synchrotron x-ray microdiffraction. *J. Appl. Cryst.* 32:1127–1133.

Mehrani, T., K. C. Wu, M. I. Morasso, J. T. Bryan, L. N. Marekov, D. A. Parry, and P. M. Steinert. 2001. Residues in the 1A rod domain segment and the Linker L2 are required for stabilizing the A11 molecular alignment mode in keratin intermediate filaments. *J. Biol. Chem.* 276: 2088–2097.

Meng, J. J., S. Khan, and W. Ip. 1994. Charge interactions in the rod domain drive formation of tetramers during intermediate filament assembly. *J. Biol. Chem.* 269:18679–18685.

Meredith, R., editor. 1956. Mechanical Properties of Textile Fibres. North-Holland Publishing Co., Amsterdam, The Netherlands.

Milam, L., and H. P. Erickson. 1982. Visualization of a 21-nm axial periodicity in shadowed keratin filaments and neurofilaments. *J. Cell Biol.* 94:592–596.

Morton, W. E., and J. W. S. Hearle. 1993. Physical Properties of Textile Fibres. The Textile Institute, Manchester, UK.

O'Brien, J. P., R. Fahnestock, Y. Termonia, and K. H. Gardner. 1998. Nylons from nature: synthetic analogs to spider silk. *Adv. Mater.* 10: 1185–1194.

Parry, D. A. D. 1995. Hard alpha-keratin IF: a structural model lacking a head-to-tail molecular overlap but having hybrid features characteristic of both epidermal keratin and vimentin IF. *Proteins Struct. Funct. Genet.* 22:267–272.

Parry, D. A. D., and P. M. Steinert. 1999. Intermediate filaments: molecular architecture, assembly, dynamics and polymorphism. *Quat. Rev. Biophys.* 32:99–187.

Peters, L., and H. J. Woods. 1956. Creep and relaxation. *In* The Mechanical Properties of Textile Fibres. R. Meredith, editor. North-Holland Publishing Co., Amsterdam, The Netherlands. 171–178.

Riekel, C., M. Burghammer, and M. Müller. 2000. Microbeam small-angle scattering experiments and their combination with microdiffraction. *J. Appl. Cryst.* 33:421–423.

Rohs, R., C. Etchebest, and R. Lavery. 1999. Unraveling proteins: a molecular mechanics study. *Biophys. J.* 5:2760–2768.

Skertchly, A. R. B., and H. J. Woods. 1960. The $\alpha \rightarrow \beta$ transformation in keratin. *J. Textile Inst.* 51:T517–T527.

Spei, M. 1975. Diffraction des rayons x aux petits angles de fibres kératiniques après modification chimique et allongement. *Forsch. West.* 2455:1–55.

Spei, M., and R. Holzem. 1987. Thermoanalytical investigations of extended and annealed keratins. *Coll. Polym. Sci.* 265:965–970.

Spei, M., and H. Zahn. 1971. Small angle x-ray scattering on stretched keratin fibers. *Monatsh. Chem.* 102:1163.

Steinert, P. M., L. Marekov, R. D. B. Fraser, and D. A. D. Parry. 1993. Keratin intermediate filaments structure. Crosslinking studies yield quantitative information on molecular dimension and mechanism of assembly. *J. Mol. Biol.* 230:436–452.

Wang, H., D. A. Parry, L. N. Jones, W. W. Idler, L. N. Marekov, and P. M. Steinert. 2000. In vitro assembly and structure of trichocyte keratin intermediate filaments. A novel role for stabilization by disulfide bonding. *J. Cell Biol.* 151:1459–1468.

Wilson, G. A. 1972. Low angle x-ray diffraction studies of the effect of extension on macromolecular organisation in keratin. *Biochim. Biophys. Acta.* 278:440–449.

Wortmann, F. J., and H. Zahn. 1994. The stress/strain curve of alpha-keratin fibers and the structure of the intermediate filament. *Text. Res. J.* 64:737–743.

Zahn, H., J. Föhles, M. Nienhaus, A. Schwan, and M. Spei. 1980. Wool as a biological composite structure. *Ind. Eng. Chem. Prod. Res. Dev.* 19:496–501.